
PHONON DYNAMIC BEHAVIORS INDUCED BY AMORPHOUS INTERLAYER AT HETEROINTERFACES

A PREPRINT

Quanjie Wang

Institute of Micro/Nano Electromechanical System College of Mechanical Engineering
State Key Laboratory for Modification of Chemical Fibers and Polymer Materials Donghua University
Shanghai, 201620, China.

Jie Zhang

Institute of Artificial Intelligence
Donghua University
Shanghai, 201620, China.

Vladimir Chernysh

Department of Physical Electronics
Lomonosov Moscow State University
Russia.

Xiangjun Liu*

Institute of Micro/Nano Electromechanical System College of Mechanical Engineering
State Key Laboratory for Modification of Chemical Fibers and Polymer Materials Donghua University
Shanghai, 201620, China.
xjliu@dhu.edu.cn

June 28, 2023

ABSTRACT

Interface impedes heat flow in heterostructures and the interfacial thermal resistance (ITR) has become a critical issue for thermal dissipation in electronic devices. To explore the mechanism leading to the ITR, in this work, the dynamic behaviors of phonons passing through the GaN/AlN interface with an amorphous interlayer is investigated by using phonon wave packet simulation. It is found the amorphous interlayer significantly impedes phonon transport across the interface, and leads to remarkable phonon mode conversions, such as LA \rightarrow TA, TA \rightarrow LA, and LA \rightarrow TO conversion. However, due to mode conversion and inelastic scattering, we found a portion of high-frequency TA phonons, which are higher than the cut-off frequency and cannot transmit across the ideal sharp interface, can partially transmit across the amorphous interlayer, which introduces additional thermal transport channels through the interface and has positive effect on interfacial thermal conductance. According to phonon transmission coefficient, it is found the ITR increases with increasing of amorphous interlayer thickness L . The phonon transmission coefficient exhibits an obvious oscillation behavior, which is attributed to the multiple phonon scattering in the amorphous interlayer, and the oscillation period is further revealed to be consistent with the theoretical prediction by the two-beam interference equation. In addition, obvious phonon frequency shifts and phonon energy localization phenomena were

1 Introduction

Interface impedes heat flow in heterostructures and the interfacial thermal resistance (ITR) has become a critical issue for thermal dissipation and energy management in electronic devices, especially for high-speed and high-power electronic applications. For example, in GaN-based high-electron mobility transistors (HEMTs), it is predicted that 40% temperature rise in the channel layer is attributed to the high ITR between GaN and substrate, leading to the channel temperature over 100 °C [1]. To alleviate this issue, various approaches with interface engineering have been developed to reduce the ITR, such as inserting buffer layer to mediate the vibrational mismatch [2] [3], doping light/ isotope atoms

to redistribute the phonon energy among different modes [1] [4], and enlarging interfacial contact area to increase the thermal transport channel [5] [6]. These approaches give rise to complex interfacial phonon scattering and transmission. Deep insight into the interplay between interface microstructures and phonon dynamic behavior can provide scientific guidance for heat dissipation.

When phonons transport across a material interface, they will experience reflection, transmission, and mode conversion, meanwhile, these properties are highly interface morphology-, size-, and defects-dependent [7] [8]. To clarify the underlying physics, the acoustic mismatch model (AMM) and diffuse mismatch model (DMM) are two early empirical models that are often used to describe the phonon transmission at the interface. Although some interfacial thermal conductance (ITC, reciprocal of ITR) values have been successfully predicted using these models while most deviate significantly from the experimental works due to their limit assumptions of phonons: complete specular scattering and complete diffuse scattering. Atomistic methods, such as atomistic Green's function method and molecular dynamics (MD) method, can take into account the actual atomic structures of the interface, and based on these methods various realistic factors, such as atomic inter-diffusion [9], interface roughness [10] [11], and dislocations [12], have been demonstrated significantly affect the nanoscale thermal transport. It should be noted the transmission coefficient is obtained with atomistic methods typically as a function of frequency, which describes a collective/averaged performance of multi phonon modes with different polarizations and buries the dynamic behavior of specific phonon mode at the interface. Actually, different phonon modes perform differently in interface thermal transport. For instance, very recently, Li et al. [13] experimentally observed that distinct types of phonons at AlN/Si interface can mutual penetration forming phonon bridges across the interface, such as Si-LA/LO mode connect to AlN-TA mode, and Si-TO mode connects to AlN-TO mode. To gain insight into these deep knowledge, in this work, we resort to the phonon wave packet simulation, which can give intuitive observation of phonon scattering of specific mode and without any phonon scattering mechanism assumption, to explore the phonon dynamic behaviors crossing the heterointerface.

In realistic material interfaces, a thin (few nm) amorphous interlayer due to lattice and thermal mismatch between dissimilar materials inevitably occurs in solid-solid interfaces [14] [15]. Some studies reporting that the amorphous interlayer improves the ITC, for example, Tian et al. [16] found that the amorphous interlayer can soften the abrupt change of acoustic impedance at Si/Ge interface and bridge the vibrational mismatch between Si and Ge. However, for the majority of heterostructures, such as GaN/diamond [14], GaN/AlN [17], GaN/SiC [15], etc, the amorphous interlayer was reported to reduce the ITC significantly since amorphous material thermal conductivities are typically very low by comparison to crystals. In addition, due to structurally disordered, only propagons exhibit a propagating nature in amorphous material [18, 19, 20]. Thus, the phonon localization phenomenon was apt to occur in disordered systems, such as Si/Ge heterostructure with interface atomic diffuse [21], GaAs superlattices with randomly distributed ErAs particles [22]. For these cases, the phonon participation ratio or the exponential decay features of phonon transmission coefficients typically as an indicator to indirectly characterize the phonon/Anderson localization, however, the direct observation of phonon localization in experiments is still challenging because of the spatial resolution limitation of conventional optical phonon detection techniques and extremely weak phonon signal from localization energy [23] [24]. Although some interesting physical phenomena induced by the amorphous interlayer have been reported by theoretical simulation, such as reducing the phonon non-equilibrium near the interface [25], there are still many ambiguous issues caused by the amorphous interlayer needed to clear. For example, whether the amorphous interlayer can alter the mode character after phonon-interface scattering? Whether the interfacial phonon dynamics depends on the size of the amorphous interlayer? How the amorphous interlayer affects all phonon modes' contribution to the ITC?

To address these issues, in this work, we use GaN/AlN as a prototype system, which widely exists and plays a vital role in GaN-based power devices, to explore the dynamic behaviors of phonons at the interface with a thin amorphous interlayer by using phonon wave packet simulation. The thickness (L) of amorphous interlayer is analogous to the experimental observation in GaN/AlN heterointerface that varied from 1~3 nm [26] [27]. A phonon wave packet is initialized with a predefined frequency and polarization and allowed to propagate through the interface. The dynamic behaviors of phonons at interface are monitored by analyzing the atomic displacements and velocities in real space and reciprocal space. The phonon transmissivity is calculated by measuring the phonon energy change before and after interface scattering. To assess the effects of the amorphous interlayer on ITC, the ITCs of GaN/AlN with different interface morphologies and amorphous interlayer thickness are calculated by summation over all phonon contributions with the Landauer formula. Finally, to improve the phonon transmission, an optimized GaN/AlN interface morphology was developed via the annealing reconstruction technique, and the resulting phonon transmission and ITC were discussed.

2 Models and methods

2.1 Model introduction.

Fig. 1(a) shows the three types of GaN/AlN heterointerfaces studied in this work, sharp interface, amorphous interface, and reconstructed interface. Sharp interface is an ideal interface, which cannot be realized due to the dislocation, stress, and high temperature growth condition. Amorphous interface was attained by locally melting the interface at 4000 K and quenched to 300 K using Nose–Hoover reservoirs. Reconstructed interface is an optimized interface, which was obtained by annealing and recrystallization of the amorphous interlayer, detailed introduction for this interface will be discussed subsequently. In our simulation, both GaN and AlN are wurtzite structures and aligned in [0001] (z) direction, mimicking the experimental epitaxial condition that GaN grows on AlN [28]. The atomic interactions are described using the Stillinger-Weber (SW) potential with the parameters developed by Bere and Serra (for GaN) [29] and Lei (for AlN) [30], and the interaction between GaN and AlN at interface are created by the mixing rule. Using these potentials, the phonon spectra for GaN and AlN along the high symmetry Γ -A ([0001]) direction were calculated, as shown in Fig. 1(b), via the harmonic lattice dynamics calculations. The unfilled circles correspond to the experimental data that are obtained by Ruf (for GaN) [31] and Schwoerer (for AlN) [32] with the inelastic X-ray scattering, which indicates that the potentials we used can accurately reproduced the essential vibration properties in GaN and AlN. Because GaN and AlN have the same atomic structure and only differ in atomic mass, thus, a similar dispersion curve is observed for both materials, except that the frequency in GaN is lower than that in AlN by a factor of $\sqrt{m_{GaN}/m_{AlN}} \approx 1.4$. The lattice constants of GaN and AlN are $a_{GaN} = 3.18 \text{ \AA}$, $c_{GaN} = 5.21 \text{ \AA}$ and $a_{AlN} = 3.09 \text{ \AA}$, $c_{AlN} = 5.05 \text{ \AA}$, which give rise to a negligible lattice mismatch strain, $\chi = (a_{GaN} - a_{AlN}) / a_{GaN} = 2.8\%$.

2.2 Phonon wave packet simulations.

To investigate the dynamic behaviors of phonons at interface, the phonon wave packet simulations were performed using the LAMMPS package [33]. A wave packet is formed from a linear combination of plane waves ε of a certain polarization v and centered at a specified wave vector k . The initialized atomic displacement $u_{l,b}$ for the b th atom in the l th unit cell in a wave packet can be assigned by the following equations:

$$u_{l,b} = \frac{A}{\sqrt{m_b}} \varepsilon_{v,k_0,b}(k_0) \exp[ik_0(z_l - z_0) - \omega t] \times \exp\left[-\frac{(z_l - z_0)^2}{\xi^2}\right] \quad (1)$$

where A is the wave packet amplitude, m_b is the atomic mass of the b th atom, $\varepsilon_{v,k_0,b}$ is the eigenvector for the b th atom in a unit cell with wave vector k_0 and polarization v , ω is the angular frequency of the phonon mode, z_l is the coordinate of the l th unit cell, and ξ is the spatial extent of the wave packet. The initialized propagation velocity of the wave packet is created by the time derivative of the initialized atomic displacement. Using this equation, a Gaussian wave packet is generated centered in real space around z_0 and in reciprocal space around k_0 . Usually, a long model system is required in wave packet simulation, here the entire system length in the z -direction was chose 1100 unit cells (600 unit cells for AlN, 500 unit cells for GaN). To avoid the influence of other modes, the whole system was first carefully relaxed to make the atoms around their equilibrium positions (~ 0 K). After that, one wave packet with designated phonon properties that are extracted from the phonon dispersion curve in Fig. 1(b) is launched from the AlN side. When the wave packet encounters the interface, scattering events take place, part of phonon energy can transmit through the interface, and some is reflected back. According to the fraction of phonon energy transmitted through the interface, the phonon transmission coefficient α can be determined as follows

$$\alpha = \frac{E_{tran}}{E_{inci}} \quad (2)$$

where E_{tran} is the transmitted phonon energy, E_{inci} is the incident phonon energy. Further, using the calculated α , the mode-resolved ITC, G , can also be estimated by summation over all phonon contributions with the Landauer formula [34]

$$G = \frac{1}{(2\pi)^2} \sum_k \sum_\lambda W_k \bar{h} \omega_{\lambda k} v_{z,\lambda k} \alpha_{\lambda k} \frac{dN(\omega, T)}{dT} \quad (3)$$

where W_k is the weighting factor associated to the k -space volume, \bar{h} is the reduced Planck constant, $v_{z,\lambda k}$ is the phonon group velocity that determined by the displacement per unit time of the wave packet, $\alpha_{\lambda k}$ is the phonon transmission

coefficient that obtained from the phonon wave packet simulations, $N(\omega, T)$ is the Bose-Einstein distribution at temperature T .

Theoretically, the wave packets can be analyzed either from the real space or from the reciprocal space. Comparing to the real space, the reciprocal space can provide more information like the phonon frequency, mode splitting and conversion after interface scattering. Thus, by Fourier transform of atomic displacements, we obtained the normal coordinates (ψ) of specific wave packet after scattering in reciprocal space

$$\Psi(k, t) = \sqrt{\frac{m_b}{N}} \sum_{lb} u_{l,b}(t) \varepsilon_{b\lambda k}^* \exp[-ik(z_l - z_0)]. \quad (4)$$

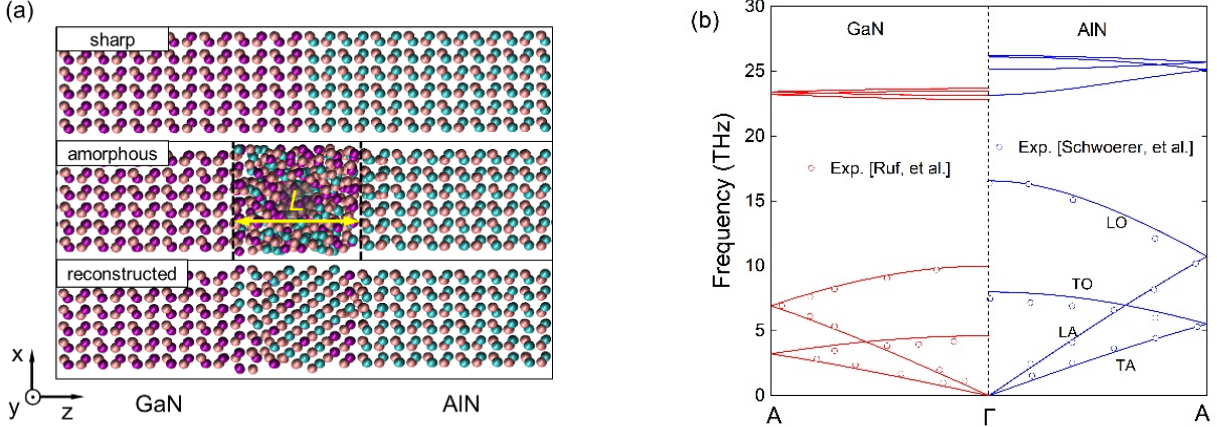


Figure 1. (a) Schematic of GaN/AlN heterostructures with sharp, amorphous, and reconstructed interfaces. (b) Phonon dispersion curves for GaN and AlN, respectively. The unfilled circles correspond to the experimental data that are obtained by Ruf (for GaN [31]) and Schwoerer (for AlN [32]) with inelastic x-ray scattering.

3 Results and discussion

3.1 Dynamic behavior of phonon passing through GaN/AlN interface

We first explored the dynamic behaviors of phonons at GaN/AlN interface with an amorphous interlayer, meanwhile, the phonon propagation at sharp interface also be displayed for comparison. As shown in Fig. 1(b), GaN and AlN have one LA branch and two degenerate TA branches. From the eigenvectors, we found that the TA mode is lateral (x - y direction) transverse-polarized and perpendicular to the wave vector. In contrast, the LA mode is not strictly axial (z direction) longitudinal-polarized and has a lateral square displacement ($<0.02\%$). This is due to the fact that the GaN and AlN both are not symmetric with respect to the (0001) plane (the x - y plane in our simulation). In this work, the TA modes are represented by the lateral atomic displacements that are averaged in the x and y directions.

Fig. 2 shows several representative snapshots of wave packets after scattering at the interface, the gray lines refer to the initialized atomic displacement in axial/lateral direction and the red lines refer to the excited atomic displacement in lateral/axial direction. For sharp interface, it is found that the energy of incident wave packet from AlN is primarily transformed into the mode with identical polarized in GaN. For example, in Fig. 2(a), a LA polarized wave packet is launched from AlN side with a frequency of 1.2 THz. After being scattered at the interface, about $\sim 97.6\%$ of the incident energy transmits into GaN side with LA polarization, and the remaining energy is reflected and maintains the LA character. Actually, there has a small amount of phonon energy, less than 0.1% of the incident energy, is converted into TA polarization and across the interface, as shown in the inset of Fig. 2(a). This unobvious LA \rightarrow TA mode conversion behavior is related to the lateral components in the phonon eigenvector of LA mode and nearly plays a negligible role in interface thermal transport. However, when the interface with an amorphous interlayer, we found that this mode conversion behavior is remarkably enhanced. As shown in Fig. 2(b), when a same LA wave packet scatters at the amorphous interface, here $L=2$ nm, the excited (transmitted and reflected) TA mode energy by LA \rightarrow TA mode conversion increases to the $\sim 4\%$ of the incident energy. And with the frequency increases, the proportion of phonon energy used for mode conversion further increases. In addition, we found that the amorphous interlayer can also convert

a portion of acoustic mode energy into optical mode, as shown in Fig. 2(c), where we launched a 3.6 THz LA wave packet. According to the propagate velocities of wave packets and the form of atom vibration (as shown in the inset of Fig. 2(c), the adjacent-layer atoms move “in-phase” referring to acoustic phonons and different types of atoms move “out-of-phase” referring to optical phonons), we verified that the reflected wave packets include two acoustic modes (LA + TA) and the transmitted wave packets include one acoustic mode (LA) and one optical mode (TO). This can be explained by the phonon spectra, where two low-frequency optical branches follow closely to the LA and TA branches. Clearly, the frequency 3.6 THz of incident wave packet just falls into the range of low-frequency TO (3.2 ~ 4.6 THz) of GaN. Therefore, the mode conversion from acoustic phonons to optical phonons is possible.

Although such mode conversion behavior has not been observed in TA (no axial component in the eigenvector) mode phonon incident at the sharp interface, it occurs at amorphous interface. As shown in Fig. 2(d), we provided one example with TA→LA mode conversion, where a 1.14 THz TA mode wave packet excited two LA modes after interface scattering. Different from the LA modes, with frequency increases, we surprisingly found a portion of high-frequency TA mode phonons that cannot transmit in sharp interface can transmit due to the existence of amorphous interlayer. Even the frequency is larger than the cut-off frequency, ~4.6 THz, of TO mode in GaN. As shown in Fig. 2(f), a TA mode phonon wave packet with a frequency of 4.8 THz scattered at amorphous interface, it is obvious there is still a considerable fraction of phonon energy that can be transmitted. Generally, when the frequency of incident wave packet beyond the cut-off frequency on the other side would be completely reflected because lacking a corresponding thermal transport channel [35]. As shown in Fig. 2(e), this same TA mode wave packet is reflected by the sharp interface completely. Thus, there are other phonon transmission channels were created at amorphous interface: TA→LA mode conversion and diffuse scattering. Meanwhile, this finding points out another reason why the AMM model cannot describe accurate phonon transmission coefficients, which neglects the mode conversion [35].

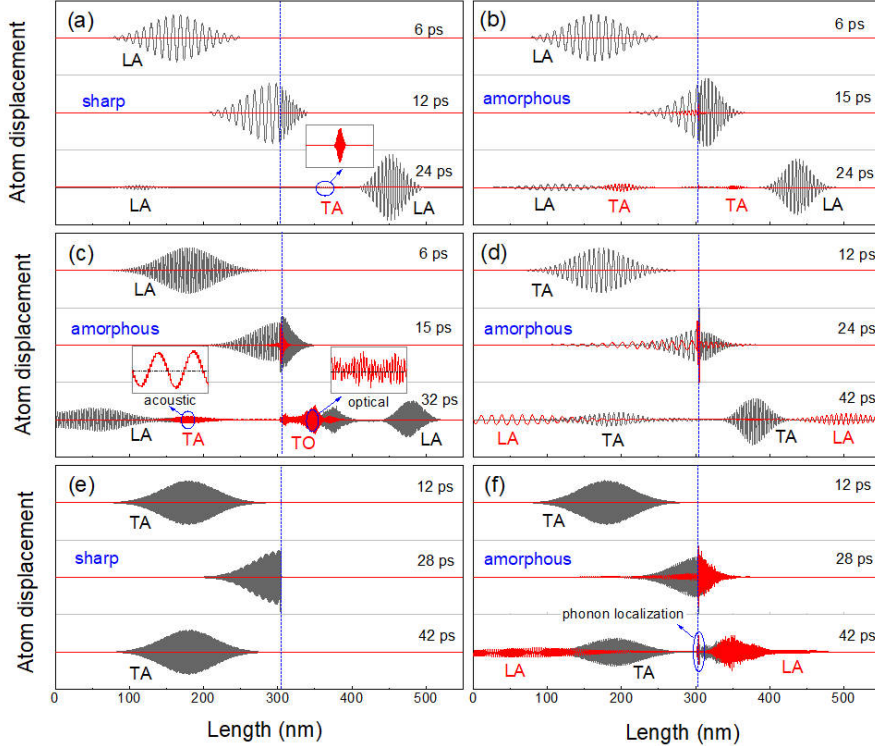


Figure 2: Snapshots of wave packets crossing the GaN/AlN interface with different polarizations, frequencies, and interfaces. The gray lines refer to the initially atom displacements, the red lines refer to the excited atom displacements after phonon-interface scattering. (a) LA, $\omega=1.2$ THz, sharp interface. (b) LA, $\omega=1.2$ THz, amorphous interface. (c) LA, $\omega=3.6$ THz, amorphous interface ($L=2\text{nm}$). (d) TA, $\omega=1.14$ THz, amorphous interface. (e) TA, $\omega=4.8$ THz, sharp interface. (f) TA, $\omega=4.8$ THz, amorphous interface ($L=2\text{nm}$). The inset in Fig. 4(a) shows the excited TA polarized phonon wave packet. The inset in Fig. 4(c) shows the form of atom vibration in different wave packets. The inset in Fig. 4(f) refers to the localized phonon around the interface.

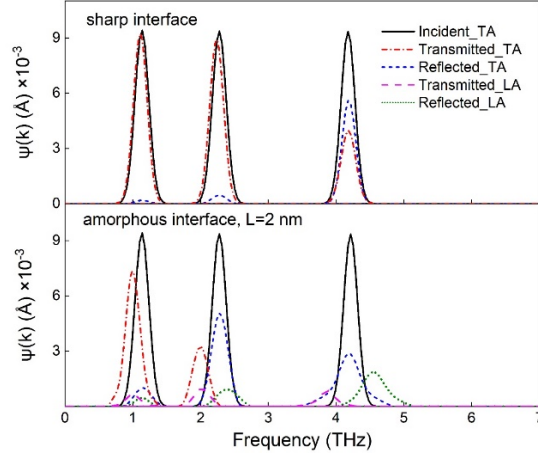


Figure 3: The normal coordinates of wave packets in reciprocal space after the interface scattering. The black lines refer to the incident TA modes, the dotted lines refer to transmitted and reflected phonon modes.

Besides the contribution from mode conversion and diffuse scattering, inelastic scattering probably occur as phonons pass through the amorphous interlayer, resulting in part high-frequency phonons being scattered into multiple lower frequency phonons and then transmitted.

To verify it, we analyzed the frequency of wave packets after scattering at sharp and amorphous interfaces, respectively, by Fourier transform of atom displacement. As shown in Fig. 3, we choose three TA mode wave packets with different frequencies of 1.14 THz, 2.28 THz, and 4.1 THz. The central location for each peak corresponds to the frequency of wave packet, and the magnitude of peak equals to the amplitude and scales quadratically ($E(k) \propto \psi^2(k)$) with the energy of wave packet. The transmitted and reflected wave packets are represented by the dotted lines. For sharp interface, it is found that the transmitted and reflected wave packets have almost the same frequency as the original incident wave packets, indicating the phonon transport process at sharp interface is completely elastic. However, when the interface with an amorphous interlayer, an obvious frequency shift occurred especially for the transmitted wave packets. For example, for an incident TA wave packet with 1.14 THz, the frequency of the transmitted TA wave packet shifts to ~ 1 THz. As we all known, the elastic process does not involve frequency conversion, thus, the frequency shift here results from the inelastic scattering. Similar inelastic scattering behaviors with wave packet simulation have also been observed in Si/Ge [36] and Si/SiO₂ [37] interfaces. It should be noted that, as the incident frequency increases, such as at 4.1 THz, either reflected or transmitted wave packet was found to span a broader frequency or wave vector range. This can be understood by the superposition principle of waves. Theoretically, one wave packet is a linear combination of plane waves that with a certain polarization and centered at a specified wave vector. Hence, the broadening of frequency means additional phonon modes that result from inelastic scattering are participating in building wave packets.

3.2 Interfacial phonon transmission

By recording the transmitted phonon energy, we further assessed the effects of the amorphous interlayer on phonon transmission. As shown in Fig. 4(a-b), the phonon transmission coefficients of LA and TA modes as a function of frequency and amorphous interlayer thickness ($L = 1$ nm, 2 nm, and 3 nm). For sharp interface, the phonon transmission coefficients show a smooth decrease with an increase in frequency. In particular, transmission coefficient changes continuously even at the cut-off frequency of LA and TA branches of GaN, presumably because of the continuity in the LA-LO and TA-TO dispersion curves. As expected from the analysis of the dispersion curves, the transmission coefficients of LA and TA attenuate to zero at ~ 9.5 THz and ~ 4.6 THz, respectively. However, when the interface has an amorphous interlayer, the phonon transmission coefficient of LA and TA fluctuates and declines sharply with the increase of frequency because of the enhanced phonon Umklapp scattering. And with thickness L increases, phonon scattering will be occurred in a broader spatial region, which results in a shorter phonon mean free path, hence the phonon transmission shows a further decrease. According to equation (3), the reduction of phonon transmission will lead to a negative effect on interface thermal transport.

For TA mode, as mentioned above we found that the amorphous interlayer leads to some unexpected scattering outcomes, where some phonons cannot transmit in sharp interface can transmit. This anomalous finding can also be confirmed by the TA mode phonon transmission in Fig. 4(b), in which the transmission coefficient of high-frequency (>4 THz) TA phonons exceeds the sharp interface. Meanwhile, in this high-frequency range, it is noted that the phonon transmission

curves flatten out and gradually became insensitive with the frequency. This phenomenon can be interpreted by the specular-diffuse scattering model [38], when the phonon wavelength is much smaller than the thickness of amorphous interfacial layer, the fraction of phonon specular scattering at interface will dramatically decrease even vanish. Therefore, the flattening of the trend is largely attributed to the full-diffusion effect, which results in the memory of the incident phonon lost. In Fig. 4(b), we observed that the transmission coefficient of TA phonon ultimately converges to $0.3\sim 0.5$, which approaches the DMM that predicts $\sim 50\%$ transmission [39], thus is a typical phonon diffusion result.

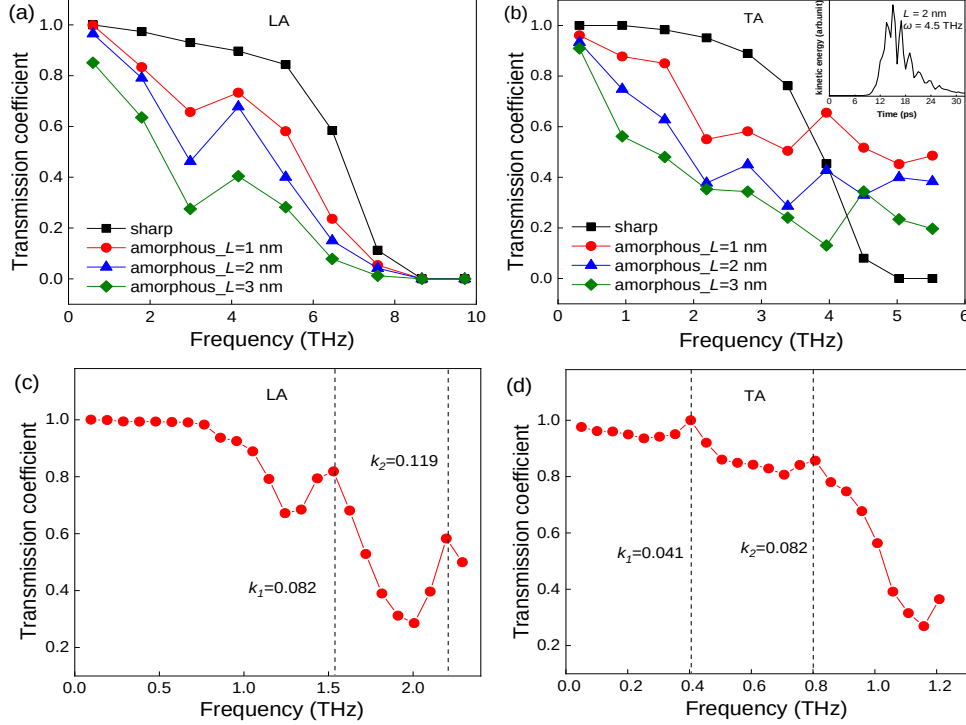


Figure 4: The energy transmission coefficients as a function of phonon frequency. (a) LA and (b) TA mode energy transmission coefficients for different interface morphologies and amorphous layer thickness. The low-frequency (a) LA and (b) TA energy transmission coefficients at amorphous interface with $L=8$ nm. The inset in (b) shows the kinetic energy evolution in the amorphous layer ($L=2$ nm) when the wave packet crosses the interface.

3.3 Phonon localization in amorphous interlayer

Another noteworthy thing is that the convergent TA mode transmission coefficient in the high-frequency region decreases with the increase of the amorphous interlayer thickness. Apart from the increased Umklapp scattering, phonon localization was revealed to be another significant impact factor. As shown in Fig. 2(f), an evident spatially localized phonon energy was trapped in the amorphous interlayer, and the fraction of the localized energy was found to increase with the increase of the thickness of the amorphous interlayer. Similar energy localization has also been reported previously in composition graded Si/Ge [23] interface and disordered Si [40] surface. Their studies suggested that the fluctuation of wave speed caused by the non-uniform mass density of the amorphous layer is an important factor of phonon localization. Theoretically, when the wave packet enters the amorphous interlayer, it cannot be supported by the disordered structure and will excite some random vibrational modes in amorphous interlayer, which are called locons or localized resonant modes [20]. Thus, part of incident wave packet energy will be converted into these random vibrational modes, and then be slowly emitted in the form of a high-frequency lattice ripple. This process can be confirmed by monitoring the kinetic energy evolution in the amorphous interlayer, as shown in the inset of Fig. 4(b), where we recorded the kinetic energy variation in the amorphous interlayer ($L=2$ nm) before and after a TA mode ($\omega=4.5$ THz) wave packet passed through the interface. We find that the kinetic energy in the amorphous interlayer first increases rapidly as the wave packet enters the amorphous interlayer and then decays gradually through a re-emission process. Even through the wave packet crossing and moving away from the interface, we found there is still about $\sim 0.46\%$ of total incident energy holding inside the amorphous interlayer in the form of localized phonons or quasi-standing waves. Since localization virtually “immobilizes” phonons and makes them non-conducting, namely,

these phonons lose their nature as heat carriers. Hence, we conclude that the phonon localization in the amorphous interlayer will aggravate heat accumulation and further decay the efficiency of energy dissipation in devices.

3.4 Phonon interference induced by the amorphous interlayer

As aforementioned, the phonon transmission coefficient fluctuates and shows an apparent oscillation behavior when the wave packets pass through the amorphous interlayer, as shown in Fig. 4(a-b). This is likely due to an interference effect. Since the amorphous interlayer actually generates two interfaces: AlN/interlayer interface and interlayer/GaN interface, which lead to the multiple scattering of incident wave packet. Specifically, when an incident wave packet hits on the AlN/interlayer interface, a portion of wave packet energy is transmitted while the other is reflected. The transmitted wave packet soon reaches the interlayer/GaN interface, producing transmitted and reflected wave packets again. These two reflected wave packets may overlap and therefore induce interference. To verify if the oscillatory behavior of transmission coefficient is caused by phonon interference, we compare the transmission coefficients from wave packet simulation with the values from the two-beam interference analytical equation [41],

$$I = I_1 + I_2 + 2\sqrt{I_1 I_2} \cos(2kL + \varphi_0), \quad (5)$$

where I is the intensity of the interference signal, i.e., the transmitted wave packet energy in our simulations; I_1 and I_2 are reflections at the two interfaces, respectively; φ_0 is initial phase of the interference, L is the thickness of the amorphous interlayer, and k is the wave vector of wave packet. Because the two adjacent interference maxima have a phase difference of 2π , thus, the interference period t_p can be defined as

$$t_p = k_{v,n+1} - k_{v,n} = \frac{\pi}{L}, \quad (6)$$

where $k_{v,n+1}$ and $k_{v,n}$ are the center wave vectors of two adjacent peaks in the interference spectrum. Obviously, the interference period t_p is inversely proportional to the thickness of the amorphous interlayer. Considering high-frequency phonon with high possibility of diffuse scattering, which can lead to decoherence of phonons and then make the observation of wave behavior challenging. Thus, to have a better understanding, we enlarged the thickness of amorphous interlayer to 8 nm, and recalculated the phonon transmission coefficient with a wave vector range from $0.01 \times (2\pi/c_{\text{AlN}})$ to $0.2 \times (2\pi/c_{\text{AlN}})$. Correspondingly, by substituting $L=8$ nm into equation (6), the interference period with theoretical prediction is 0.39 nm^{-1} .

Fig. 4(c-d) shows the calculated phonon transmission coefficients at this low-frequency range, it is clear that the transmission coefficient of both LA and TA modes exhibits an evident oscillatory behavior. According to the center frequencies (ω_1, ω_2) of the two adjacent peaks in Fig. 4(c-d), we obtained their corresponding wavevectors (k_1, k_2) with the help of phonon dispersion curves in Fig. 1(b). Here, for LA mode, $k_1=0.82 \text{ nm}^{-1}$ and $k_2=1.19 \text{ nm}^{-1}$, similarly, for TA mode, $k_1=0.41 \text{ nm}^{-1}$ and $k_2=0.82 \text{ nm}^{-1}$. Further, the oscillatory periods for LA and TA are determined as 0.37 nm^{-1} and 0.41 nm^{-1} , respectively, which agree well with the interference period 0.39 nm^{-1} in theoretical predication. Therefore, we conclude that the oscillatory behavior of transmission coefficient was ascribed to the phonon interference effect and the maxima and minima of transmission coefficient are the result of destructive and constructive interferences, respectively.

3.5 Interfacial thermal conductance

To further quantify the phonon contributions at different interface morphologies, the mode-resolved ITCs were obtained with the calculated phonon transmission coefficients and Landauer formula. Strictly speaking, the cumulative ITC should be a summation of phonon contribution over the entire first Brillouin zone [19] [34]. Here we simplified the calculation and quantified the phonons contribution perpendicular to the interface direction (Γ - A direction), which has been demonstrated to be the major channel in GaN/AlN interfacial thermal transport [42] [43]. Specifically, the Brillouin zone was discretized with a $40 \times 40 \times 40$ k -point grid, in which the 40 k -points along the Γ - A direction were used. Fig. (5) shows the ITC contributions from each phonon branch by equation (3) for sharp as well as amorphous interfaces. For sharp interface, LA and TA modes contribute $\sim 50\%$ of the ITC across the interface, respectively. Compared with the sharp interface, the ITC with an amorphous interlayer shows a pronounced reduction, and with the increase of L nearly monotonically decreases. When $L=3$ nm, the ITC decreased by $\sim 54\%$ from $176 \text{ MWm}^{-2}\text{K}^{-1}$ to $82 \text{ MWm}^{-2}\text{K}^{-1}$. The decreased trend and magnitude in ITC are comparable to recent reports [9], in which the GaN/AlN interface with a compositional diffusion interlayer.

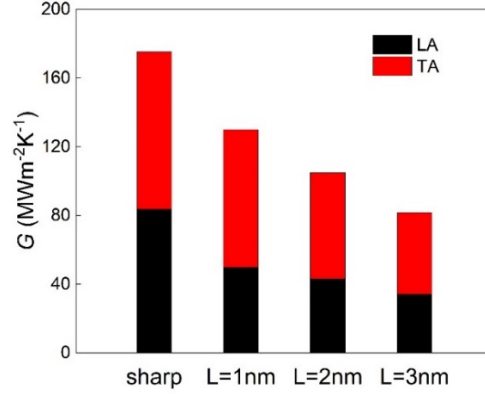


Figure 5: Mode-resolved ITCs for sharp and amorphous ($L = 1, 2,$ and 3 nm) GaN/AlN interfaces.

3.6 Interface morphology optimization

Given the remarkable ITR induced by the amorphous interlayer, we further optimized the interface morphology via annealing reconstruction technique. Recently, the effectiveness of this method has been experimentally demonstrated in heterogenous GaN/SiC interface [15]. Fig. 1(a) shows the reconstructed GaN/AlN interface, in which we found that the amorphous interlayer converted into rocksalt phase instead of the initialized wurtzite phase after annealing. This finding has also been demonstrated in first-principle calculation [44] and experimental observation [45], resulting from the state of the AlN rocksalt phase being more stable and energy being more favorable in comparison to its wurtzite phase. Taking $L=2$ nm as an example, we calculated the phonon transmission coefficient for reconstructed interface using the wave packet simulations, as shown in Fig. [6]. And the amorphous interface with the same interlayer thickness also is displayed for comparison. Compared to the amorphous interface, the phonon transmission coefficients of the reconstructed interface at low- and mid-frequency regions have a remarkable improvement, indicating the reconstructed interlayer reduced the phonon scattering and then lead to a relatively large amount of phonon energy across the interface. Further, we also quantified the phonon contribution to ITC, as shown in Fig. 6(c), it is found that the ITC improved by $\sim 21\%$ after annealing treatment. It should be noted that compared with the sharp interface, there still exists a large gap. This difference mainly attributed to two factors. First, the intrinsic thermal conductivity of rocksalt AlN is much lower than that of the wurtzite phase. Using ab initio simulation, Shulumba *et al.* [44] reported that the thermal conductivity of the rocksalt phase ($81 \text{ Wm}^{-1}\text{K}^{-1}$) of AlN was only a quarter of the wurtzite phase ($320 \text{ Wm}^{-1}\text{K}^{-1}$) due to the influence of phonon inelastic scattering. Second, the rocksalt phase altered the original crystallographic orientation, which can also cause additional phonon scattering and then suppress the phonon propagation forward.

4 Conclusions

In this work, using phonon wave packet simulation, we studied the phonon dynamic behaviors at GaN/AlN interface with an amorphous interlayer. We found that the amorphous interlayer impedes the phonon transport, and the resulting phonon transmission coefficient exhibits an obvious frequency and amorphous layer thickness dependency. Compared to the sharp interface, complicated phonon scattering events, such as mode conversion, frequency shift (or inelastic scattering), phonon interference, and phonon localization, were occurred when phonons pass through the interface. Due to the multiple scattering of phonons in the amorphous interlayer, the phonon transmission coefficient exhibits an oscillation behavior, and the oscillation period is consistent with the theoretical prediction using the two-beam interference equation. In addition, it is interesting to find that the high-frequency TA phonons transmissivity in the amorphous interface is abnormally higher than that across the sharp interface due to the mode conversion and inelastic scattering, which facilitate the redistribution of phonon energy. Finally, to aid phonon transmission, we further optimized the interface morphology by annealing reconstruction technique, which leads to an obvious improvement of the phonon transmission coefficients in low- and mid-frequency regions. Correspondingly, the ITC increases by 21% when $L=2$ nm. Our study provides a deep understanding of the dynamic behaviors of phonons across the heterointerface and gives important insight into the physical origin of ITR.

ACKNOWLEDGMENTS

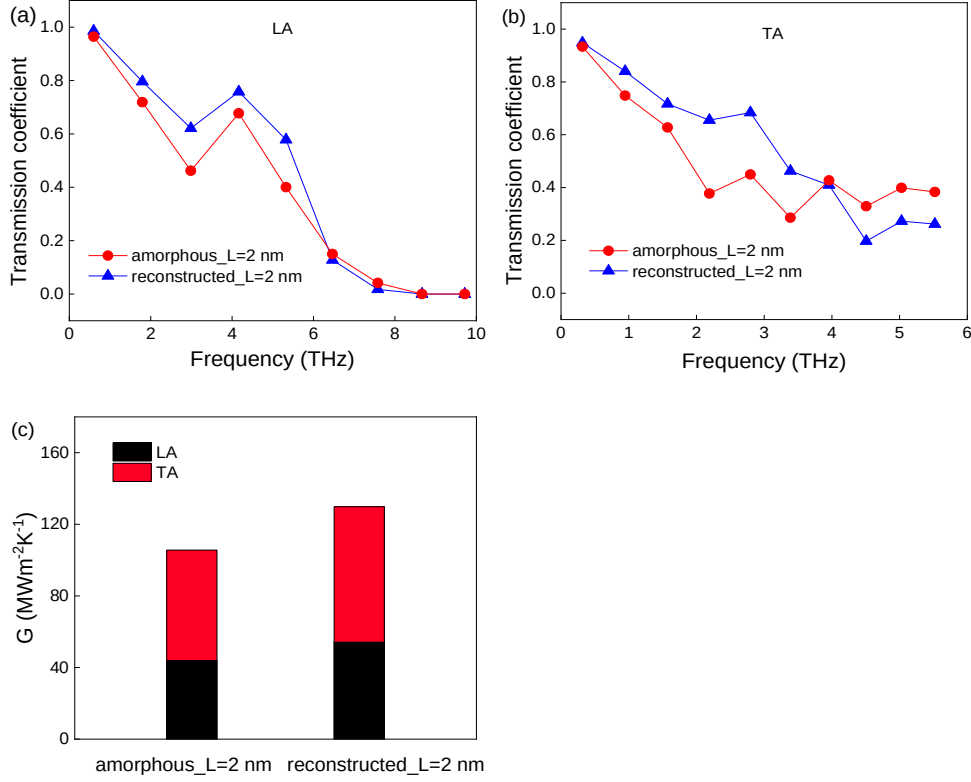


Figure 6: (a) LA and (b) TA mode energy transmission coefficients for amorphous and reconstructed interfaces. (c) Mode-resolved ITCs for amorphous and reconstructed interfaces.

The authors gratefully acknowledge the financial support from National Natural Science Foundation of China (Grant No. 52150610495 and Grant No. 52206080), the Shanghai Committee of Science and Technology (Grant No. 21TS1401500), and the Shanghai Municipal Natural Science Foundation (Grant No. 22YF1400100).

References

- [1] Eungkyu Lee and Tengfei Luo. Thermal transport across solid-solid interfaces enhanced by pre-interface isotope-phonon scattering. *Applied Physics Letters*, 112(1):011603, 2018.
- [2] Ming Hu, Xiaoliang Zhang, Dimos Poulikakos, and Costas P Grigoropoulos. Large “near junction” thermal resistance reduction in electronics by interface nanoengineering. *International journal of heat and mass transfer*, 54(25-26):5183–5191, 2011.
- [3] Eungkyu Lee and Tengfei Luo. The role of optical phonons in intermediate layer-mediated thermal transport across solid interfaces. *Physical Chemistry Chemical Physics*, 19(28):18407–18415, 2017.
- [4] Ruiyang Li, Kiarash Gordiz, Asegun Henry, Patrick E Hopkins, Eungkyu Lee, and Tengfei Luo. Effect of light atoms on thermal transport across solid–solid interfaces. *Physical Chemistry Chemical Physics*, 21(31):17029–17035, 2019.
- [5] Lei Tao, Sreeprasad Theruvakkattil Sreenivasan, and Rouzbeh Shahsavari. Interlaced, nanostructured interface with graphene buffer layer reduces thermal boundary resistance in nano/microelectronic systems. *ACS Applied Materials & Interfaces*, 9(1):989–998, 2017.
- [6] Eungkyu Lee, Teng Zhang, Taehee Yoo, Zhi Guo, and Tengfei Luo. Nanostructures significantly enhance thermal transport across solid interfaces. *ACS applied materials & interfaces*, 8(51):35505–35512, 2016.
- [7] Xiaobo Li and Ronggui Yang. Size-dependent phonon transmission across dissimilar material interfaces. *Journal of Physics: Condensed Matter*, 24(15):155302, 2012.
- [8] Xiaobo Li and Ronggui Yang. Effect of lattice mismatch on phonon transmission and interface thermal conductance across dissimilar material interfaces. *Physical Review B*, 86(5):054305, 2012.

- [9] Xinyu Liu, Quanjie Wang, Renzong Wang, Sheng Wang, and Xiangjun Liu. Impact of interfacial compositional diffusion on interfacial phonon scattering and transmission in gan/aln heterostructure. *Journal of Applied Physics*, 133(9), 2023.
- [10] Xiao Wang Zhou, Reese E Jones, Christopher James Kimmer, John C Duda, and Patrick E Hopkins. Relationship of thermal boundary conductance to structure from an analytical model plus molecular dynamics simulations. *Physical Review B*, 87(9):094303, 2013.
- [11] Quanjie Wang, Jie Zhang, Yucheng Xiong, Shouhang Li, Vladimir Chernysh, and Xiangjun Liu. Atomic-scale surface engineering for giant thermal transport enhancement across 2d/3d van der waals interfaces. *ACS Applied Materials & Interfaces*, 2023.
- [12] Hongkun Li, Riley Hanus, Carlos A Polanco, Andrea Zeidler, G Koblmüller, Yee Kan Koh, and Lucas Lindsay. Gan thermal transport limited by the interplay of dislocations and size effects. *Physical Review B*, 102(1):014313, 2020.
- [13] Yue-Hui Li, Rui-Shi Qi, Ruo-Chen Shi, Jian-Nan Hu, Zhe-Tong Liu, Yuan-Wei Sun, Ming-Qiang Li, Ning Li, Can-Li Song, Lai Wang, et al. Atomic-scale probing of heterointerface phonon bridges in nitride semiconductor. *Proceedings of the National Academy of Sciences*, 119(8):e2117027119, 2022.
- [14] Zhe Cheng, Fengwen Mu, Luke Yates, Tadatomo Suga, and Samuel Graham. Interfacial thermal conductance across room-temperature-bonded gan/diamond interfaces for gan-on-diamond devices. *ACS applied materials & interfaces*, 12(7):8376–8384, 2020.
- [15] Fengwen Mu, Zhe Cheng, Jingjing Shi, Seongbin Shin, Bin Xu, Junichiro Shiomi, Samuel Graham, and Tadatomo Suga. High thermal boundary conductance across bonded heterogeneous gan–sic interfaces. *ACS applied materials & interfaces*, 11(36):33428–33434, 2019.
- [16] Zhiting Tian, Keivan Esfarjani, and Gang Chen. Enhancing phonon transmission across a si/ge interface by atomic roughness: First-principles study with the green’s function method. *Physical Review B*, 86(23):235304, 2012.
- [17] Quanjie Wang, Xujun Wang, Xiangjun Liu, and Jie Zhang. Interfacial engineering for the enhancement of interfacial thermal conductance in gan/aln heterostructure. *Journal of Applied Physics*, 129(23):235102, 2021.
- [18] Kiarash Gordiz and Asegun Henry. Phonon transport at interfaces: Determining the correct modes of vibration. *Journal of Applied Physics*, 119(1):015101, 2016.
- [19] Kiarash Gordiz and Asegun Henry. Phonon transport at interfaces between different phases of silicon and germanium. *Journal of Applied Physics*, 121(2):025102, 2017.
- [20] Wu-Xing Zhou, Yuan Cheng, Ke-Qiu Chen, Guofeng Xie, Tian Wang, and Gang Zhang. Thermal conductivity of amorphous materials. *Advanced Functional Materials*, 30(8):1903829, 2020.
- [21] Yuxiang Ni, Honggang Zhang, Song Hu, Hongyan Wang, Sebastian Volz, and Shiyun Xiong. Interface diffusion-induced phonon localization in two-dimensional lateral heterostructures. *International Journal of Heat and Mass Transfer*, 144:118608, 2019.
- [22] Jonathan Mendoza and Gang Chen. Anderson localization of thermal phonons leads to a thermal conductivity maximum. *Nano letters*, 16(12):7616–7620, 2016.
- [23] Honggang Zhang, Haoxue Han, Shiyun Xiong, Hongyan Wang, Sebastian Volz, and Yuxiang Ni. Impeded thermal transport in composition graded sige nanowires. *Applied Physics Letters*, 111(12):121907, 2017.
- [24] Chaitanya A Gadre, Xingxu Yan, Qichen Song, Jie Li, Lei Gu, Huaixun Huyan, Toshihiro Aoki, Sheng-Wei Lee, Gang Chen, Ruqian Wu, et al. Nanoscale imaging of phonon dynamics by electron microscopy. *Nature*, 606(7913):292–297, 2022.
- [25] Qinshu Li, Fang Liu, Song Hu, Houfu Song, Susu Yang, Hailing Jiang, Tao Wang, Yee Kan Koh, Changying Zhao, Feiyu Kang, et al. Inelastic phonon transport across atomically sharp metal/semiconductor interfaces. *Nature communications*, 13(1):4901, 2022.
- [26] Anna Spindlberger, Dmytro Kysylychyn, Lukas Thumfart, Rajdeep Adhikari, Armando Rastelli, and Alberta Bonanni. Cross-plane thermal conductivity of gan/aln superlattices. *Applied Physics Letters*, 118(6):062105, 2021.
- [27] Y Zheng, Manvi Agrawal, Nethaji Dharmarasu, K Radhakrishnan, and Shashank Patwal. A study on gasi interdiffusion during (al) gan/aln growth on si by plasma assisted molecular beam epitaxy. *Applied Surface Science*, 481:319–326, 2019.
- [28] HV Stanchu, AV Kuchuk, PM Lytvyn, Yu I Mazur, Y Maidaniuk, M Benamara, Shibin Li, S Kryvyi, VP Kladko, AE Belyaev, et al. Strain relaxation in gan/aln superlattices on gan (0001) substrate: Combined superlattice-to-substrate lattice misfit and thickness-dependent effects. *Materials & Design*, 157:141–150, 2018.

- [29] Antoine Béré and Anna Serra. Atomic structure of dislocation cores in gan. *Physical Review B*, 65(20):205323, 2002.
- [30] HP Lei. *Molecular Dynamics and First Principle Investigations of Dislocations and Quantum Wells in III-Nitride Semiconductors*. PhD thesis, Doctoral thesis, Caen University, 2009.
- [31] T Ruf, J Serrano, M Cardona, P Pavone, M Pabst, M Krisch, M D’astuto, T Suski, I Grzegory, and M Leszczynski. Phonon dispersion curves in wurtzite-structure gan determined by inelastic x-ray scattering. *Physical review letters*, 86(5):906, 2001.
- [32] M Schwoerer-Böhning, AT Macrander, M Pabst, and P Pavone. Phonons in wurtzite aluminum nitride. *physica status solidi (b)*, 215(1):177–180, 1999.
- [33] Steve Plimpton. Fast parallel algorithms for short-range molecular dynamics. *Journal of computational physics*, 117(1):1–19, 1995.
- [34] Xingfei Wei and Tengfei Luo. A phonon wave packet study of thermal energy transport across functionalized hard-soft interfaces. *Journal of Applied Physics*, 126(1):015301, 2019.
- [35] Bin Liu and Vladimir Ivanovich Khvesyuk. Analytical model for thermal boundary conductance based on elastic wave theory. *International Journal of Heat and Mass Transfer*, 159:120117, 2020.
- [36] Bowen Deng, Aleksandr Chernatynskiy, Marat Khafizov, David H Hurley, and Simon R Phillpot. Kapitza resistance of si/sio2 interface. *Journal of Applied Physics*, 115(8):084910, 2014.
- [37] Lin Sun and Jayathi Y Murthy. Molecular dynamics simulation of phonon scattering at silicon/germanium interfaces. 2010.
- [38] Cheng Shao, Qingyuan Rong, Nianbei Li, and Hua Bao. Understanding the mechanism of diffuse phonon scattering at disordered surfaces by atomistic wave-packet investigation. *Physical Review B*, 98(15):155418, 2018.
- [39] Arun Majumdar and Pramod Reddy. Role of electron–phonon coupling in thermal conductance of metal–nonmetal interfaces. *Applied Physics Letters*, 84(23):4768–4770, 2004.
- [40] Cheng Shao, Qingyuan Rong, Ming Hu, and Hua Bao. Probing phonon–surface interaction by wave-packet simulation: Effect of roughness and morphology. *Journal of Applied Physics*, 122(15):155104, 2017.
- [41] Zhi Liang, Thomas E Wilson, and Pawel Keblinski. Phonon interference in crystalline and amorphous confined nanoscopic films. *Journal of Applied Physics*, 121(7):075303, 2017.
- [42] Zhiguo Wang, Xiaotao Zu, Fei Gao, William J Weber, and Jean-Paul Crocombette. Atomistic simulation of the size and orientation dependences of thermal conductivity in gan nanowires. *Applied physics letters*, 90(16):161923, 2007.
- [43] Wenjing Ju, Zhongyuan Zhou, and Zhiyong Wei. Anisotropic thermal transport property of defect-free gan. *AIP Advances*, 6(6):065328, 2016.
- [44] Nina Shulumba, Zamaan Raza, Olle Hellman, Erik Janzén, Igor A Abrikosov, and Magnus Odén. Impact of anharmonic effects on the phase stability, thermal transport, and electronic properties of aln. *Physical Review B*, 94(10):104305, 2016.
- [45] Michael Pravica, Neelanjan Bhattacharya, Yu Liu, John Robinson, Wing-Sing Au, Teruyasu Mizoguchi, Zhenxian Liu, and Yuming Xiao. High pressure infrared and x-ray raman studies of aluminum nitride. *physica status solidi (b)*, 250(4):726–731, 2013.